ZIBELINE INTERNATIONAL™ PUBLISHING

ISSN: 2521-0890 (Print)
ISSN: 2521-0491 (Online)
CODEN: GBEEB6

Geological Behavior (GBR)

DOI: http://doi.org/10.26480/gbr.01.2025.36.45

RESEARCH ARTICLE

APPLICATION OF GEOELECTRICAL RESISTIVITY AND GROUND PENETRATING RADAR SIGNATURES IN DELINEATING HYDROCARBON POLLUTED SOIL IN OGONI, NIGER DELTA, NIGERIA

Stanley Uchechukwu Eze[a*], Okezie Uchegbulam[b], Rotimi Salami[c], Saleh A. Saleh[d]

[a] Department of Applied Geology, Olusegun Agagu University of Science and Technology, Okitipupa, Nigeria
[b] Department of Applied Geophysics, Federal University of Petroleum Resources, Effurun, 330102, Nigeria
[c] Department of Applied Geophysics, Olusegun Agagu University of Science and Technology, Okitipupa, Nigeria
[d] Department of Petroleum Engineering and Geosciences, Petroleum Training Institute, Effurun, Nigeria
[*]Corresponding Author Email: su.eze@oaustech.edu.ng

ARTICLE DETAILS

Article History:

Received 15 April 2025
Revised 13 May 2025
Accepted 18 May 2025
Available online 17 June 2025

ABSTRACT

The study investigated the importance and image behavior of integrated geophysical methods in mapping contaminant spread beneath the surface of a pollution site in Ogoniland, Southern Nigeria. Electrical Resistivity Tomography (ERT) and Ground Penetrating Radar (GPR) techniques constrained by Vertical Electrical Sounding (VES) data were employed to investigate the electrical properties of hydrocarbon-contaminated soils that resulted from recent oil spills/leakage into the environment. Five (5) ERT and GPR lines and twenty-nine (29) VES data were acquired at the spill site. Basically, the electrical signatures from the resistivity measurements were able to image the subsurface layers and the associated contamination zone. GPR equally imaged the subsurface stratigraphy to a depth of 10.0 m beneath the surface. The interpretation of the five (5) ERT data showed consistency in the resistivity structure indicative of contaminant plumes with anomalously high electrical resistivity in the range of 1000-10,000 Ωm, a possible indication of hydrocarbon contamination. On the GPR radargram, regions of high electrical resistivities were in agreement with reduced GPR reflection behavior (shadow zones) and were limited to the near surface of the surveyed areas. Vertical electrical sounding delineated layers with high resistivity predominantly within the second and fourth geoelectric layers within pollution depths of 2.4 m and 11.9 m, respectively. As a result, the underground aquifer, relatively between 7.5 and 10.5 m, has been infiltrated by hydrocarbons. It can be seen from the study that geoelectric measurements on the surface can describe the distribution of hydrocarbon resistive zones as well as their conductive behavior that may be linked with the biodegradation of oil spills in the subsurface. Thus, the employment of these integrated methods for contaminant monitoring, hydrogeologic studies and remediation planning reduced the uncertainties, and they are of extensive relevance in mapping the geological behavior of polluted soils in contamination sites.

KEYWORDS

Hydrocarbon Contamination; Electrical Resistivity Tomography; Ground Penetrating Radar; Conductivity.

1. INTRODUCTION

The search for energy resources as a result of increased demand in the world has led to vigorous exploration and exploitation of fossil fuels beneath the surface. These exploitation activities often lead to degradation of the environment due to accidents, equipment failure, and outright sabotage. The Niger Delta is a high producing hydrocarbon region in southern Nigeria with the attendant negative impact on the environment (Obasi and Balogun, 2001; Tamuno and Felix, 2006). The release of a limited size of oil into the environment is known as a slick while a large-scale release is termed a spill (Ivanov and Zatyagalova, 2008). The cumulative dynamics of these incidences on the earth's surface and beneath the surface often affect the soil, groundwater, vegetation, etc (Patel et al., 2019). Pollution in soil as a result of leakage of petroleum products from pipes has introduced organic pollutants in soils of the affected area (Rosales et al., 2012). Soil and underground water are important natural resources that humans depend on for survival; any negative shift in their composition and neutral PH behavior will equally impact negatively on the local population.

Electrical Resistivity Tomography (ERT) and Ground Probing Radar (GPR) offer acceptable results for near surface investigations of pollution sites and characterizations (Eze et al., 2021). Near surface survey is in the neighbourhood of 30m beneath the surface, and the ground is conductive due to mineral water present, different types of rocks, and self-potentials of the ground as a result of dissolved salts. The resistivity of rock depends on water content, the resistivity of the water, the content of clay, and metallic mineral content (Benard, 2003).

The resistivity method is being used at sites polluted by organic materials (Atekwana et al., 2000). Freshly spilled hydrocarbons are extremely good insulators and show high electrical resistivity behavior (Delaney et al., 2001). Matured ($\geq$ 20 years) hydrocarbon-contaminated sites predict low resistivity behavior that coincides with contamination as opposed to the long-established and proven high resistivity behavior (Park, 2001; Werkema et al., 2003). This model considers high conductivity to mineral weathering resulting from an abundance of microbial redox processes in the subsoil.

Ground Probing Radar is a near surface, high-image quality geophysical

Quick Response Code	Access this article online	
	Website: www.geologicalbehavior.com	DOI: 10.26480/gbr.01.2025.36.45

Cite The Article: Stanley Uchechukwu Eze, Okezie Uchegbulam, Rotimi Salami, Saleh A. Saleh (2025). Application of Geoelectrical Resistivity and Ground Penetrating Radar Signatures in Delineating Hydrocarbon Polluted Soil in Ogoni, Niger Delta, Nigeria. *Geological Behaviour 9(1): 36-45.*

method that utilizes low-to-high frequency pulsed electromagnetic (e-m) waves to image the subsurface. A GPR unit sends e-m energy into the subsurface, which is returned, bent or scattered back to the surface depending on the target it hits. Typically, GPR images to depths of about 10m, but can penetrate to depths of hundreds of meters in a very poor conductive media such as ice or salt (Everett, 2013). The attenuation of the radar signal is a function of the electrical conductivity of materials in the subsurface. Objects with higher conductivities lead to greater reduction of the signal. Dielectric constant is based on the ease with which a material becomes polarized by the introduction of an electric field. Air has a value of one, while for fresh water and seawater it can get up to 80. GPR reflections result from contrasts in the dielectric constant of materials. The contrast in permittivity is directly proportional to the reflected signal.

The velocity equation can be used to estimate the depth of targets in the subsurface.

$$D = \frac{CT}{2\sqrt{\varepsilon_r}} = \frac{V_m T}{2} \quad (1)$$

(USACE, 1995)

where

V_m = material's velocity

C = velocity of light in a vaccum

ε_r = relative electric permittivity

T = two-way travel time in nanoseconds

The study area map is shown in Figure 1.

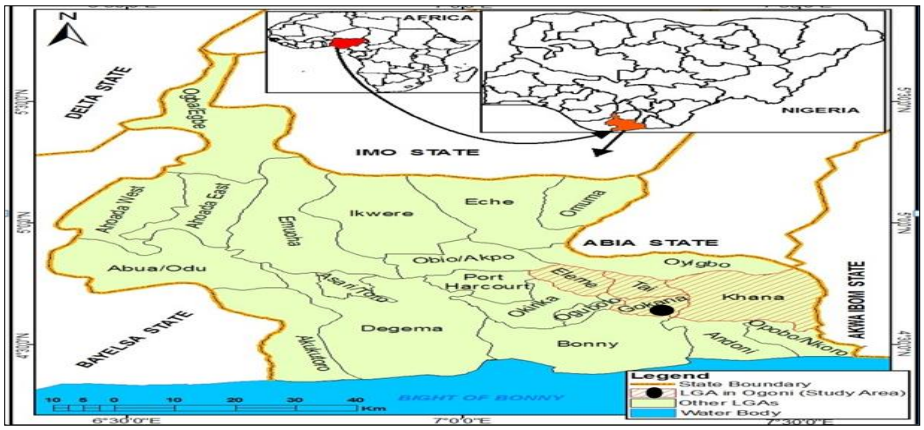

Figure 1: Map showing Gokana in Ogoni, Rivers State, Nigeria (Source: Bodo and Lekpa, 2018).

A highly conductive contaminated groundwater plumes has been mapped using GPR (Pomposiello, 2004; Porsani et al., 2004). Matured petroluem products form a ring of conductive groundwater and soil around them and are detected by a GPR antenna (Atekwana et al., 2002; Bradford, 2003; Sauck et al., 1998). Studies by researchers suggest that GPR can assist in monitoring remediation by following the trail of differences in the conditions of subsurface (Paterson, 1997; Bradford, 2004; Lane et al., 2004).

In the Niger Delta region, successfully incorporated GPR to characterize hydrocarbon spill site (Oyinkuro and Wariebi, 2017). They reported that freshly spilled hydrocarbon is easily detected by GPR, while mature spills are usually masked by conductive clayey soils and saline environment. The damage done to Ogoni land as a result of oil spillage is so massive that United Nations did a report on the area (UNDP, 2006). There is therefore the need to routinely carry out geophysical investigation in the area to monitor the state of the soil which will also reveal the condition of groundwater, vegetation and general ecosystem of that environment.

2. Geology of The Area

The spill site is located at Kegbara-Dere (K-Dere) community in Ogoniland, Gokana local government area, Rivers State. Gokana is located between latitudes $4^0\ 12^1$ and $4^0\ 50^1$ North of the equator and between longitudes $7^0\ 20^1$ to $7^0\ 35^1$ East of the Greenwich meridian (Figure 1). It situates on the Gulf of Guinea and it is about Fifty-four (54) kilometers from Port Harcourt metropolis (Okonny, 2002). Located in Rivers State, Nigeria, the inhabitants of Ogoni land are of ethnic minorities occupying an area of around 404 square miles that forms part of the Eastern Niger Delta. According to the study, the region is located between latitudes 4°.05' and 4°.20' North and longitudes 7°.10' and 7°.30' East (Agbonofo, 2009).

Rich alluvial soil and a meander of streams and creeks, which are the results of both fluvial and marine sedimentation and were strengthened since the upper Cretaceous period, some 66 million years ago, are features that promote the KegbaraDere community in Ogoniland. The region's geology is identical to that of the Niger Delta. Many workers have done extensive studies on the geology of the region, stratigraphy, and structural system (Asseez 1989; Ideozu et al. 2018; Doust and Omatsola 1990). From top to bottom Benin, Agbada, and Akata formations are part of the stratigraphy of the Niger Delta Basin (Figure 2). Brief summaries of these formations' emblematic sections can be found in publications like (Doust and Omatsola 1990; Giadom et al. 2015). Akata formation is mostly made up of layers of sand and sea-level shale, while it's subsurface is made up of sand and dark gray shale. This stratum is estimated to be about 7,000 meters thick (Giadom et al. 2015). A sequence of sandstone and shale deposits make up the upper Agbada formation. Shale is present in the lower part, although the top half is primarily composed of sand with a small bit of shale. Benin layer is about 3,700 m thick and are mostly uncovered near the coast, but are covered in many areas with lean layers of laterite of varying thickness. It has been identified as recent water-bearing sand (Doust and Omatsola 1990; Uchegbulam and Ayolabi 2014), and this lithostratigraphic unit (Figure 2) contains all of the aquifers in the delta region.

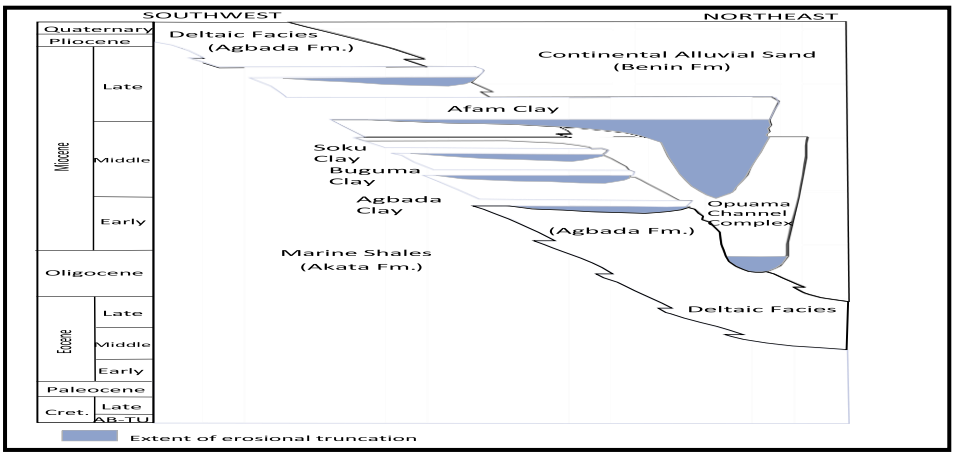

Figure 2: The three stratigraphic units of the Niger Delta (modified from Doust and Omatsola 1990).

3. Methodology and Field Design

In this study investigation of the subsurface contaminant distribution was accomplished with the use of geophysical field investigation utilizing the 2-dimensional electrical resistivity, vertical electrical sounding (VES), and ground penetrating radar (GPR) techniques to map and delineate the extent of hydrocarbon contamination at the pollution site.

3.1 Electrical Resistivity Tomography

The resistivity imaging covered 200 x 100 m^2 rectangular grid at the spill site, and twelve (12) 2D traverse lines were acquired at the spill site. Each of the traverse lines were performed using the hybrid 2-D Wenner-Schlumberger electrode array, with 21 stainless electrodes with electrode spacings of 5 m and 10 m along the 100 m and 200 m profile lengths respectively (Pazdirek and Blaha 1996). The Wenner-Schlumberger array was used for n-factors 1 through 9. The ratio of the distance between the potential pairs P1–P2 and the initial current and potential electrodes C1–P1 is the n-factor for this array. After careful examination of the depth of inquiry and the array's sensitivity to both horizontal and vertical variations in resistivity pattern, this array is the most suitable if both good data quality and vertical and horizontal sensitivity are required according to (Bery, 2016).

The ERT survey was carried out with the use of multi-electrode Resistivity Meter of type ABEM SAS-4000 comprising 21 electrodes to improve speed in field data collection. The grid lines were designed to cut across the observed pool of oil spills at the pollution site.

After conducting the 2D ERT survey, twenty-nine (29) vertical electrical soundings (VES 1-29) were collected at the spill site utilizing the Schlumberger procedure. The maximum current electrode spacing utilized was shifted from 300 m to 500 m so as to probe into shallow and profound layers. The reason for the VES study is to evaluate the condition of shallow aquifers to discover patterns in hydrocarbon pollution with regard to depth. This will guide future groundwater production within the area for sustainable development.

3.2 Ground Probing Radar (GPR)

GPR investigations were achieved by utilizing the Geophysical Survey Systems, GSSI SIR-3000 instrument with a 100MHz bistatic antennae recording at sample rate of 512 nanoseconds (ns) and were done primarily along 2D ERT traverse lines 1, 2, 4, 5, and 11 respectively at the spill site (Figure 3). The GPR traverse lines were recorded as file numbers 015, 009, 014, 013, and 018 along ERT lines 1, 2, 4, 5, and 11 respectively. Average filter of three-scan was applied to the data and consequently slight horizontal smoothing was accomplished. It is worthy to point out that this investigation used constant gain settings rather than automatic gain control (AGC) or other gain variations along the profile lines. A constant gain setting aids in the identification of minor fluctuations in amplitude of signals which may be eliminated with the employment of an AGC filter. Electromagnetic properties of some earth materials is shown in Table 1

Table 1: Electromagnetic Properties of Some Earth Materials (After USACE, 1995)

Material	Dielectric Constant	Velocity of Wave (m/Ns)	Conductivity (mS/m)
Clays	5-40	0.06	2-1,000
Silts	5-30	0.07	1-100
Limestone	4-8	0.12	0.5-2
Sand (wet)	20-30	0.06	0.1-1
Granite	4-6	0.13	0.01-1
Sand (dry)	3-5	0.15	0.01
Ice	3-4	0.16	0.01
Fresh water	80	0.033	0.5
Sea water	80	0.01	3,000
Air	1	0.3	0

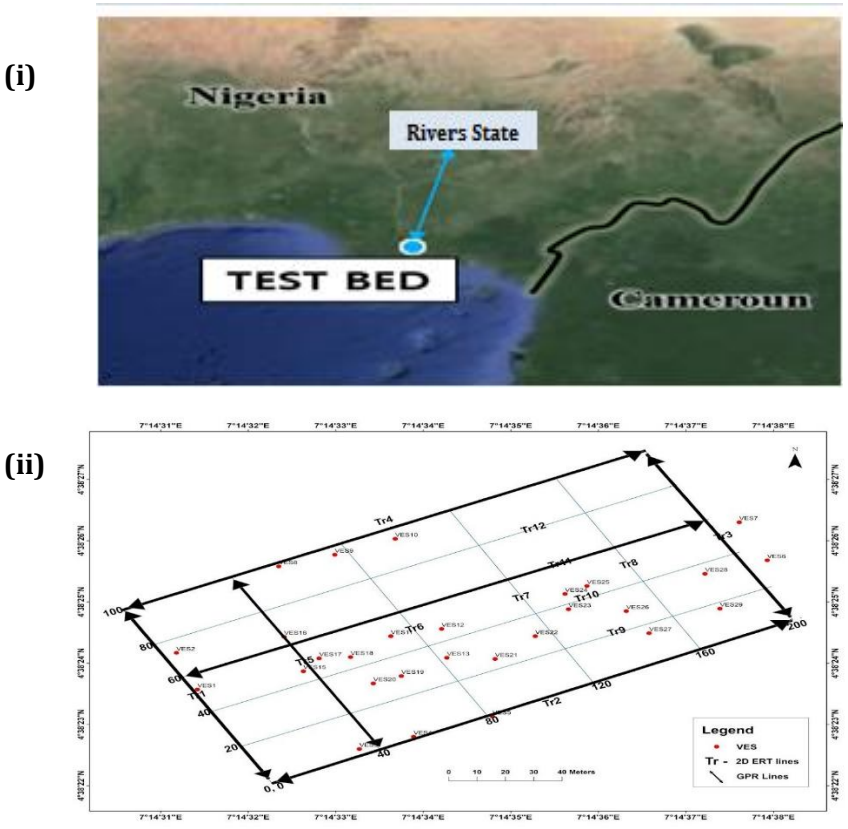

Figure 3: (i) Location map of the study area showing the spill site (test bed) **(ii)** Base map of data acquisition showing the 2D ERT and GPR survey lines acquired at the experimental test site and VES sampling locations.

3.3 Data processing and inversion

The Earth-Imager 2-D inversion application was utilized to process and invert the 2-D resistivity data (AGI, 2013), to realize the 2D resistivity-depth sections for traverses 1, 2, 4, 5, and 11. Topographic elevation difference between electrodes was adjusted during post-processing using the elevations and GPS data collected in the field.

Vertical Electrical Sounding data were processed to get the resistivity model curves and were achieved by manually curve-fitting the VES data. Thereafter, were curve-fitted to the auxiliary and master curves. The obtained layer parameters were entered into the WinResist software to obtain the 1-dimensional resistivity models (layer's resistivity and thickness). Hydrocarbon-contaminated geoelectric layers which typically have high apparent resistivity weights were then defined based on these models.

The processing of GPR data were achieved through the use of ReflexW and the results expressed in 2D format called radargrams. The radargrams revealed the geometry, quality, and type of target objects and layers within the subsurface. The GPR-radar sections were converted to depth using a velocity of 100 ns/m for better correlation with 2D ERT sections.

4. Results

4.1 2D ERT and GPR Results

The 2D resistivity-depth section and the corresponding radargram section along traverses 1, 2, 4, 5, and 8 are shown in Figures 4 a, b, 5 a, b, 6 a-d, 7 a, b, and 8 a, b respectively.

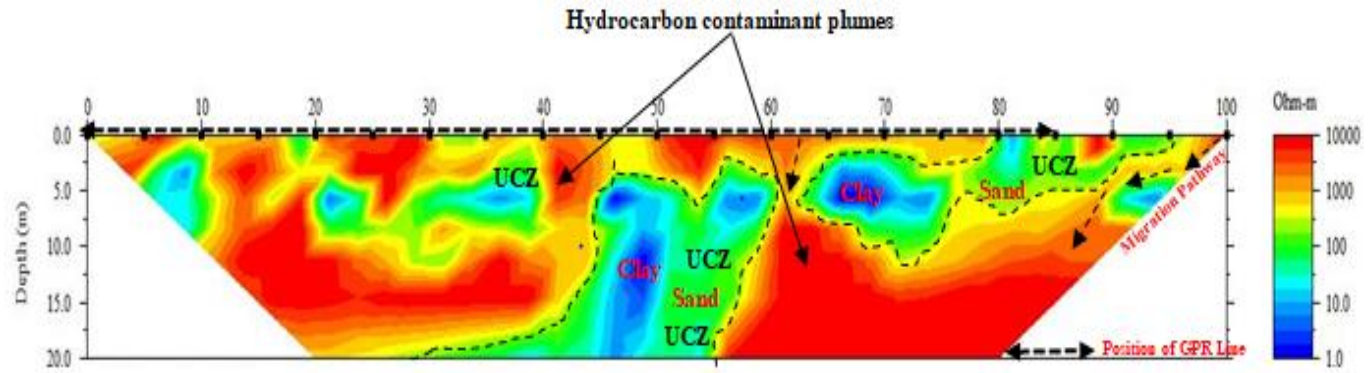

Figure 4(a): 2D W-S array Inverted resistivity section for Traverse-1 (**UCZ**: Uncontaminated zone)

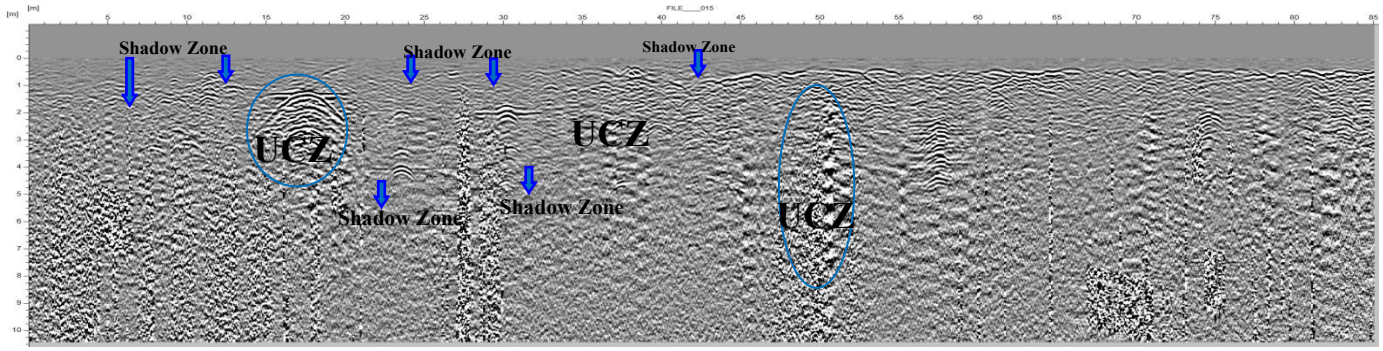

Figure 4(b): GPR-015 Radargram section from 0-85 m along 2D ERT traverse-1 (**UCZ**: Uncontaminated zone)

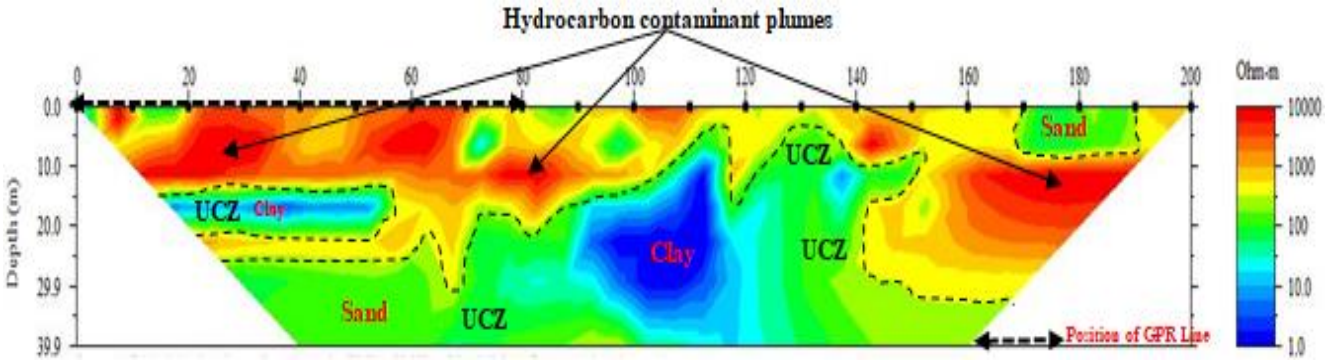

Figure 5(a): 2D W-S array Inverted resistivity section for Traverse-2 (**UCZ**: Uncontaminated zone)

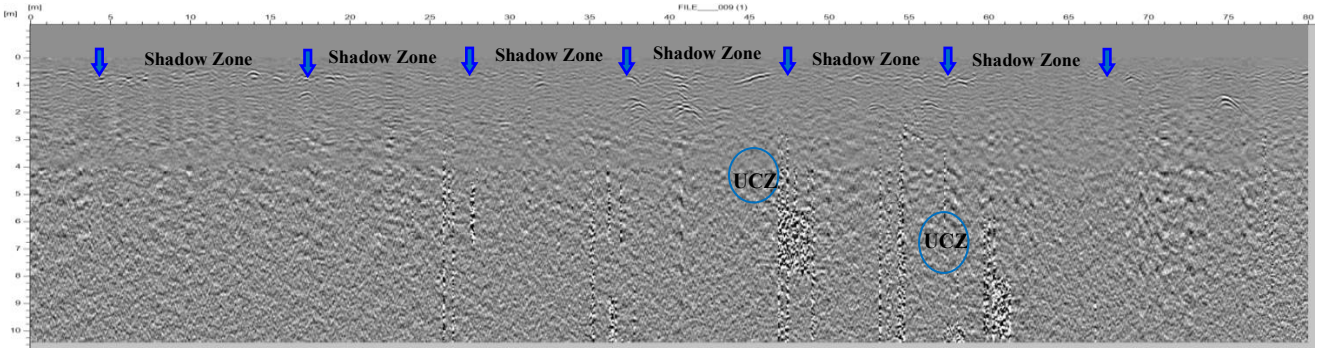

Figure 5(b): GPR-009 Radargram section from 0-80 m along 2D ERT traverse-2 (**UCZ**: Uncontaminated zone)

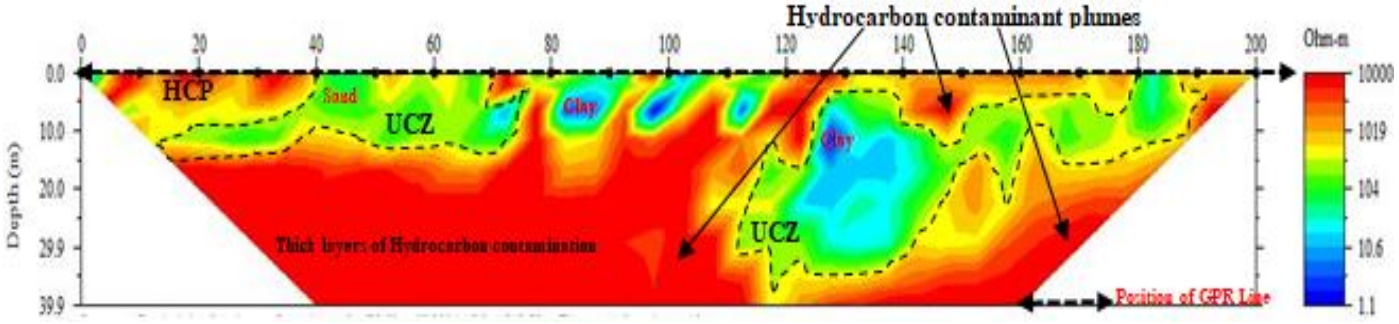

Figure 6(a): 2D W-S array Inverted resistivity section for Traverse-4 (**UCZ**: Uncontaminated zone)

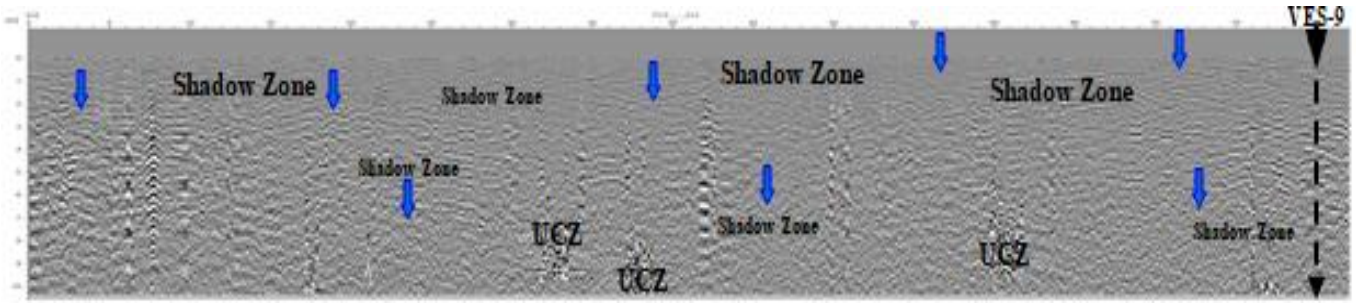

Figure 6(b): GPR-014 Radargram section from 0-82 m along 2D ERT traverse-4 (**UCZ**: Uncontaminated zone)

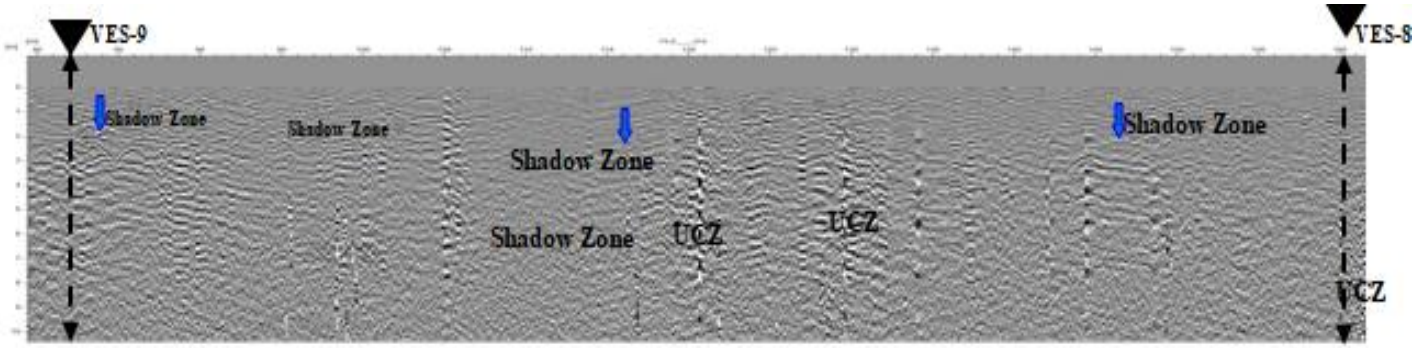

Figure 6(c): GPR-014 Radargram section from 82-160 m along 2D ERT traverse-4 (**UCZ**: Uncontaminated zone)

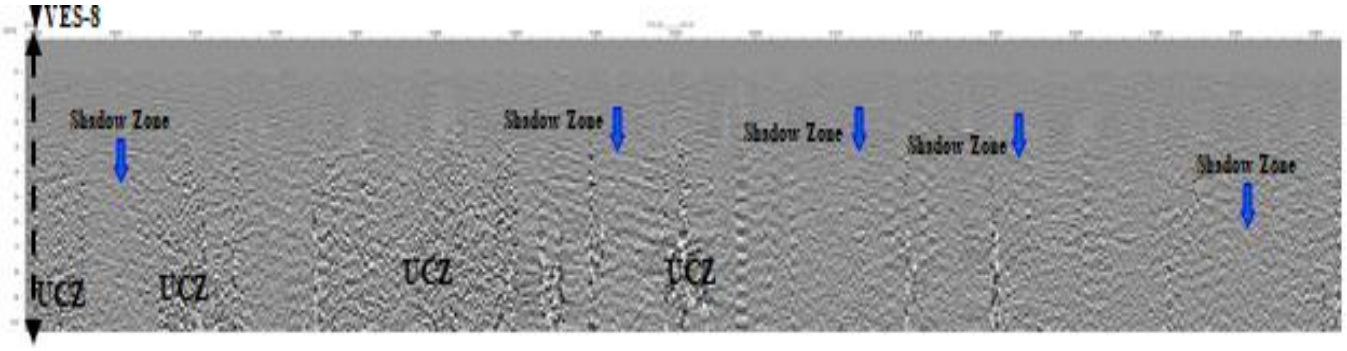

Figure 6(d): GPR-014 Radargram section from 160-240 m along 2D ERT traverse-4 (**UCZ**: Uncontaminated zone)

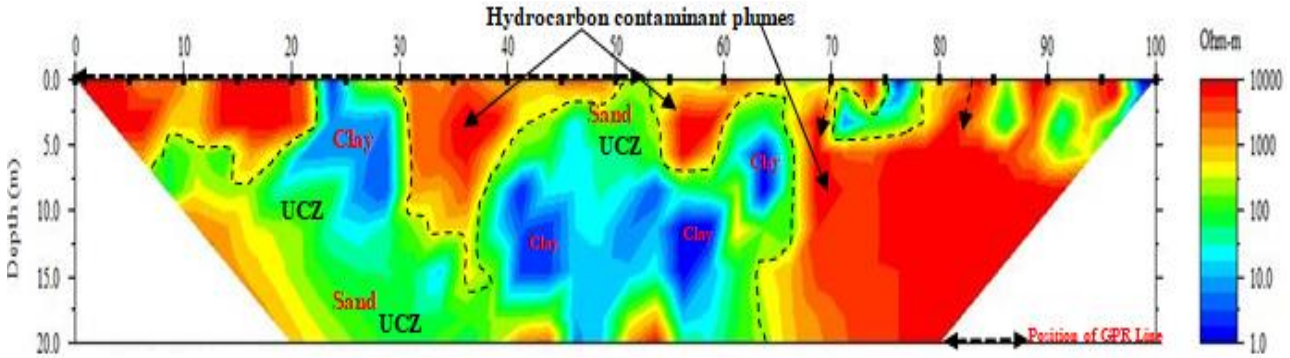

Figure 7(a): 2D W-S array Inverted resistivity section for Traverse-5 (**UCZ**: Uncontaminated zone)

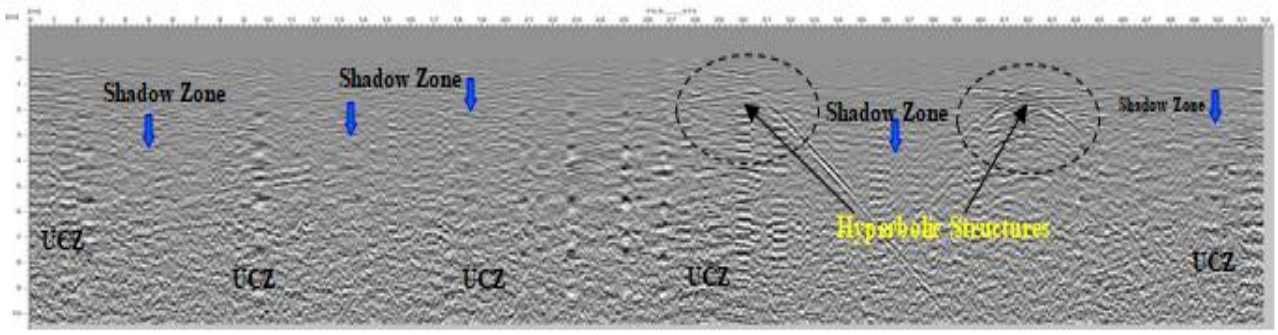

Figure 7(b): GPR-013 Radargram section from 0-52 m along 2D ERT traverse-5 (**UCZ**: Uncontaminated zone)

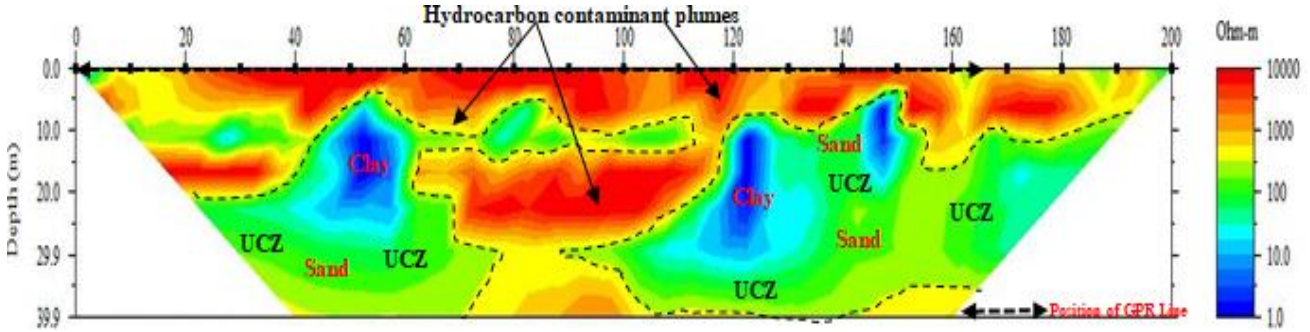

Figure 8(a): 2D W-S array Inverted resistivity section for Traverse-11 (**UCZ**: Uncontaminated zone)

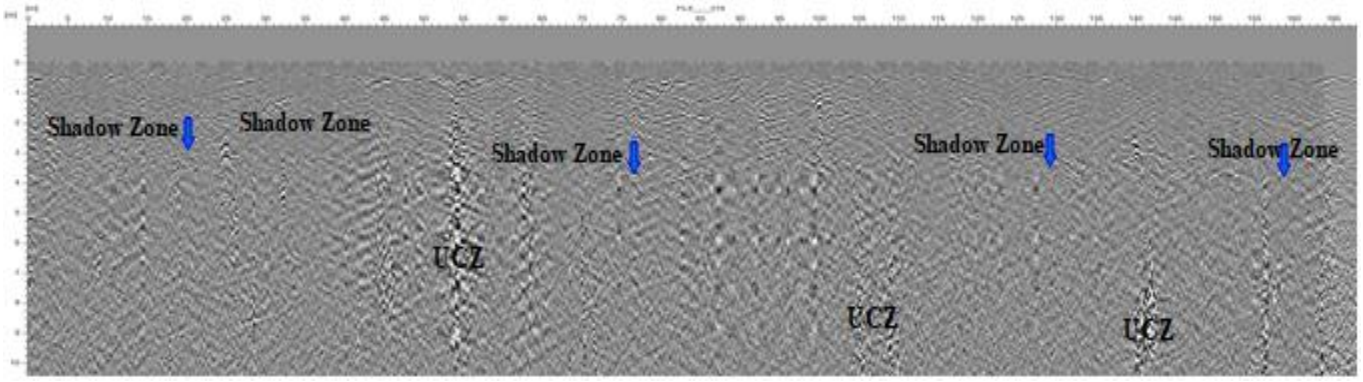

Figure 8(b): GPR-019 Radargram section from 0-165 m along 2D ERT traverse-11 (**UCZ**: Uncontaminated zone)

4.2 VES results

Table 2 presents an overview of the resistivity values for the VES model that were derived from the 1-D resistivity inversion. The geoelectric layers that have been invaded by hydrocarbon contaminant plume are indicated by the red asterisk (Table).

Table 2: Summary of VES results, showing layer resistivity, thicknesses, depths, RMS error, and hydrocarbon contaminated geo-electric layers.

VES No.	Layer resistivity ($\rho_1/\ \rho_2/\ \rho_3/.../\ \rho_n$)	Layer thickness ($h_1/\ h_2/h_3/.../\ h_n$)	Layer depth ($d_1/\ d_2/d_3/.../\ d_n$)	RMS Error (%)	Inference
VES 1	848.9/47.0/7.8/49.7	0.7/2.4/10.9/-	0.7/3.1/14.0/-	2.6	
VES 2	944.0/71.9/10.3/3.8	0.7/2.9/17.0/-	0.7/3.6/20.6/-	2.0	
VES 3	5241.2/477.6/88.2/23.3	0.8/3.9/17.7/-	0.8/4.7/22.4/-	2.1	
VES 4	16694.4/*918.8/131.8/570.9/40.6	0.7/1.7/4.9/14.0/-	0.7/2.4/7.3/21.3/	2.6	*Plume invaded layer
VES 5	7468.2/*918.7/147.3/377.4/69.7	0.8/2.1/8.8/28.6/-	0.8/2.9/11.7/40.3/-	2.5	*Plume invaded layer
VES 6	11940.2/*3438.4/*1093.1/*7425.3	0.9/3.2/18.9/-	0.9/4.2/23.1/-	2.5	*Plume invaded layer
VES 7	3428.4/883.2/154.2/*1342.6/95.1	0.5/3.6/7.5/19.8/-	0.5/4.1/11.6/31.3/-	4.5	*Plume invaded layer
VES 8	1301.9/72.6/25.9/136.4	0.7/3.8/19.0/-	0.7/4.5/23.5/-	2.1	
VES 9	5098.3/700.2/205.0/*1478.5	0.6/2.7/17.3/-	0.6/3.4/20.7/-	2.5	*Plume invaded layer
VES 10	4343.1/723.8/160.7/30.1	0.8/6.5/25.7/-	0.8/7.3/33.0/-	2.4	

Table 2 (cont): Summary of VES results, showing layer resistivity, thicknesses, depths, RMS error, and hydrocarbon contaminated geo-electric layers.

VES 11	10788.8/*3805.3/679.5/*2886.4/315.0	1.1/4.5/13.1/27.8/-	1.1/5.5/18.6/46.4/-	3.3	*Plume invaded layer
VES 12	20762.7/*7241.3/*2856.2/*12025.3/*2259.8	0.8/1.9/6.2/28.7/-	0.8/2.6/8.8/37.5/-	2.5	*Plume invaded layer
VES 13	6101.5/853.0/199.3/43.6	0.9/7.2/20.7/-	0.9/8.1/28.8/-	3.4	
VES 14	10271.6/*2992.8/578.0/143.4	1.1/3.4/28.0/-	1.1/4.4/32.4/-	3.3	*Plume invaded layer
VES 15	13068.7/*2592.0/549.3/179.8	1.0/4.2/25.0/-	1.0/5.2/30.2/-	3.2	*Plume invaded layer
VES 16	4015.6/*1138.9/393.5/*1649.9/167.7	0.5/2.4/6.9/18.6/-	0.5/3.0/9.9/28.5/-	3.6	*Plume invaded layer
VES 17	13835.6/*3690.6/709.6/178.0	1.0/4.7/31.6/-	1.0/5.7/37.2/-	2.2	*Plume invaded layer
VES 18	4635.5/623.7/164.4/45.1	0.9/7.8/28.2/-	0.9/8.8/37.0/-	2.3	
VES 19	11956.3/*1903.3/433.4/97.7	0.9/5.1/26.4/-	0.9/6.0/32.4/-	2.5	*Plume invaded layer
VES 20	8537.8/*921.7/194.0/41.5	0.8/6.4/30.4/-	0.8/7.2/37.6/-	2.3	*Plume invaded layer
VES21	7233.9/467.7/137.5/21.0	0.8/6.9/30.3/-	0.8/7.8/38.0/-	2.4	
VES22	4933.3/785.0/154.3/24.0	0.7/6.5/29.2/-	0.7/7.3/36.4/-	2.5	
VES23	5396.6/688.0/190.8/45.8	0.8/6.8/28.2/-	0.8/7.6/35.8/-	2.5	
VES24	11023.8/*4768.5/*1022.0/189.8	0.9/4.2/34.6/-	0.9/5.1/39.7/-	2.2	*Plume invaded layer
VES25	25282.9/*5184.0/*1100.4/151.8	1.1/10.8/28.5/-	1.1/11.9/40.4/-	2.6	*Plume invaded layer
VES26	5584.2/645.3/145.7/42.4	1.0/6.8/26.9/-	1.0/7.8/34.7/-	3.7	
VES27	10913.5/*2890.6/577.7/106.0	1.2/4.1/20.2/-	1.2/5.3/25.5/-	2.7	*Plume invaded layer
VES28	15989.8/*2357.2/536.9/188.0	1.2/6.7/29.2/-	1.2/8.0/37.2/-	2.4	*Plume invaded layer
VES29	3424.4/647.2/169.5/45.8	1.0/7.1/27.4/-	1.0/8.1/35.5/-	2.4	

*Hydrocarbon plume contaminated layer

5. Discussion of Results

The geoelectrical signatures observed from the 2D ERT results indicate that beneath the subsurface is composed of materials of soil with a resistivity range of 1.0-10,000 Ωm, which reflects the changing extent of conductivity linked with lithological changes and type of fluid. The ERT results show resistivity spread over horizontal distances of 100 m and 200 m, with three (3) distinct ER structures in the order of 1.0-10.0 Ωm and 100-500 Ωm representing the uncontamination zone (UCZ), and an anomalously high ER structure in the order of 1000-10,000 Ωm attributed to the presence of hydrocarbon contamination (hydrocarbons have a higher ER than water). These high ER values were observed along traverse 1 (Figure 4a), traverse 2 (Figure 5a), traverse 4 (Figure 6a), traverse 5 (Figure 7a), and traverse 11 (Figure 8a).

Similarly, two-dimensional GPR-radargram sections were produced along the various traverses to correlate the 2D ERT interpretation. The field data show excellent record quality and a maximum depth of 10.0 m was imaged within the subsurface. A weak reflection attributed to attenuation that resulted in a GPR shadow zone at the near-surface was observed in all the radargrams. Reduction of GPR reflections may be related to the presence of high-resistivity contaminant plumes, which limit the effective depth of penetration of the electromagnetic waves (Sauck et al., 1998). Likewise, targets that effectively reflect the e-m energy are recognized in the records, which are fairly continuous in the radargrams and occur at approximately 8-10 m in the subsurface. It can be interpreted as the uncontaminated zone consisting of sand and clay formations due to variations in the relative permittivity of the zones. These occur at varying depths as computed in the radargrams.

In traverse-1 (Figure 4a), the 2-D ER result shows the resistivity spread over a horizontal distance of 100 m on the surface to 20.0 m deep underneath the surface. The 2-D section showed an unusually high resistivity (1000 - 10,000 Ωm) hydrocarbon contaminant plume from the surface to a depth of 20.0 m at various lateral distances. Similarly, the GPR-radargram section (Figure 4b) along this traverse, which imaged 10.0 m of the subsurface, shows shadow zones with attenuated GPR reflections as evidence for a high resistivity contamination zone attributed to infiltration of hydrocarbon plumes.

In traverse-2 (Figure 5a), the 2-D ER result shows the resistivity spread over a horizontal distance of 200 m from the surface to a depth of 39.9 m underneath the surface. The 2-D section showed unusually high resistivity (1000 - 10,000 Ωm) hydrocarbon contaminant plumes from the surface to a depth of 20.0 m and above at various lateral distances. Similarly, the GPR-radargram section (Figure 5b) along this traverse, which imaged 10.0 m of the subsurface, shows shadow zones with attenuated GPR reflections as evidence for a high resistivity contamination zone, which can be linked to the presence of hydrocarbon in the soils of the area.

In traverse-4 (Figure 6a), the 2-D ER result shows the resistivity spread over a horizontal distance of 200 m from the surface to a depth of 39.9 m underneath the surface. The 2-D section showed an unusually high resistivity (1019 - 10,000 Ωm) hydrocarbon contaminant plume from the surface to a depth of 39.9 m at various lateral distances. The GPR data along this traverse has a traverse length of 240 m. Therefore, the GPR data was reprocessed using the split-spectrum processing technique (SSP) to find the moisture ingress. The GPR signal was analyzed in splits. These signals were then analyzed individually using a statistical filter to separate the GPR signal and noise to uncover important information that connects such features as boundary, shape, and position. In addition to information on the borders and chemical composition (contaminant plume mass). The split signals for GPR-014 data consist of traverse lengths of 0-82 m (Figure 6b), 82-160 m (Figure 6c), and 160-240 m (Figure 6d). The split radargram sections improved the ratio of the strength of the signal to noise and identified the subsurface structures better than a combined radargram. In Figures 6b, 6c, and 6d, the radargram sections imaged the subsurface to a depth of 10.0 m of the subsurface and show shadow zones

with attenuated GPR reflections as evidence for a high resistivity contamination zone, which can be linked to the infiltration of a hydrocarbon plume, and uncontaminated zones.

In traverse-5 (Figure 7a), the 2-D ER result shows the resistivity spread over a horizontal distance of 100 m from the surface to a depth of 20.0 m beneath the surface. The 2-D section uncovered an unusually high resistivity (1000 - 10,000 Ωm) hydrocarbon contaminant plume from the surface to a depth of 20.0 m at various lateral distances. Similarly, the GPR-radargram section (Figure 7b) along this traverse, which imaged 10.0 m of the subsurface, shows shadow zones with attenuated GPR reflections as evidence for a high resistivity contamination zone attributed to the presence of hydrocarbon pollution. In Figure 7b, the radargram data revealed hyperbolic signatures that are important indicators of subsurface features indicative of discrete horizontal interfaces below the surface. Some shadow zones of weak signals were also identified in Figure 7b between the hyperbolic structures that are related to contaminant plumes (Sauck et al., 1998).

In traverse-11 (Figure 8a), the 2-D ER result shows the resistivity spread over a horizontal distance of 200 m from the surface to 39.9 m deep underneath the surface. The 2-D section uncovered an unusually high resistivity (1000 - 10,000 Ωm) hydrocarbon contaminant plumes from the surface to a depth of 39.9 m at various lateral distances. Similarly, the GPR-radargram section (Figure 8b) along this traverse, which imaged 10.0 m of the subsurface, shows shadow zones with attenuated GPR reflections as evidence for a high resistivity contamination zone attributed to the presence of hydrocarbon pollution.

Generally, the establishment of the five (5) 2-D apparent resistivity-depth sections (Figures 4a-8a) showed trends in the resistivity structure for hydrocarbon contamination within the depths imaged. Furthermore, the study area consists of a dominance of clay and sandy-clay materials that form the uncontaminated zones. They act as seals since they prevent the contaminants from percolating downwards due to their low permeabilities, as observed in Figures 4a to 8a. In addition, these anomalously high electrical resistivity signatures observed in this study may be linked to the escape of fluids from various underground pipelines in the area or from surface slicks or spills due to vandalization. The study area is composed of porous sand with fairly high permeability and a water table close to the surface, about 5-6 m underneath the surface. The high resistivity (≥1000 Ωm) is possible evidence that the aquifer within this area may have been infiltrated by hydrocarbons, sandy layers being the possible migration medium.

In the VES results for VES 1 to 29, a low RMS error of 2.0 % to 4.5 % was attained (Table 2). The level of hydrocarbon contamination at the spill site was assessed using the VES interpretation results, which are reported in

Table 2. From the VES interpretation, four to five geological layers were delineated beneath the surface. Using the layer characteristics, contaminated layers were identified that had a characteristic high resistivity aberration of order (ρ > 900 Ωm), which is evidence of infiltration of hydrocarbon contaminants. The resistivity of the soil is increased when oil splatters are present under the surface. For VES 4, 5, 6, 7, 9, 11, 12, 14, 15, 16, 17, 19, 20, 24, 25, 27, and 28, these low conductive zones were observed in the second and fourth geo-electric layers; nevertheless, they were mostly found in the second layer (Table 2).

Figures 9 a and b show the contaminant map of the second and fourth geo-electric layers, which was created to evaluate the level of hydrocarbon contamination in these layers. The maps demonstrate that the second and fourth layers have been totally infiltrated by hydrocarbon plumes at the spill site (contaminated areas are delineated by the red color in Figures 9 a and b). The pollution depths within the second layer lies between 2.4 m and 11.9 m of the subsurface, alongside VES 25 having the most profound pollution depth of 11.9 m (Table 2). Consequently, the underground aquifer, relatively between 7.5 and 10.5 m, has been contaminated by hydrocarbon pollution. This observation was revealed by the 2D ERT model and confirmed by the GPR.

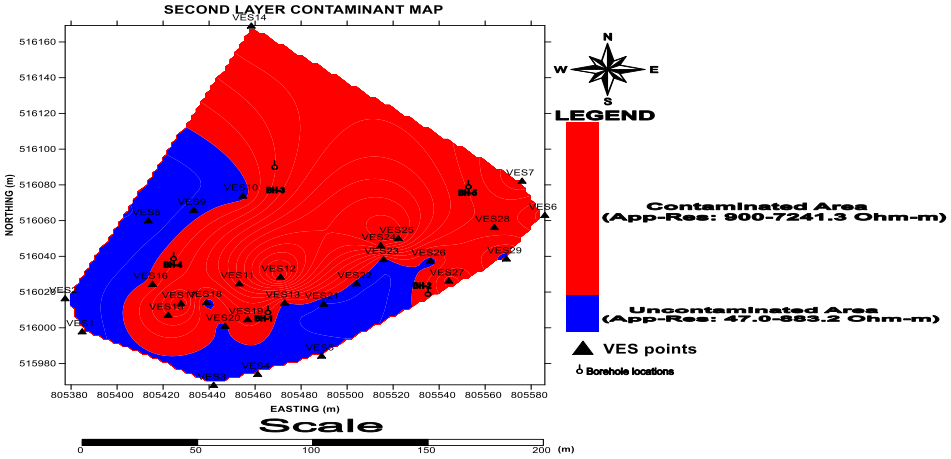

Figure 9a Spill site: Second layer contaminant map for VES 1-29.

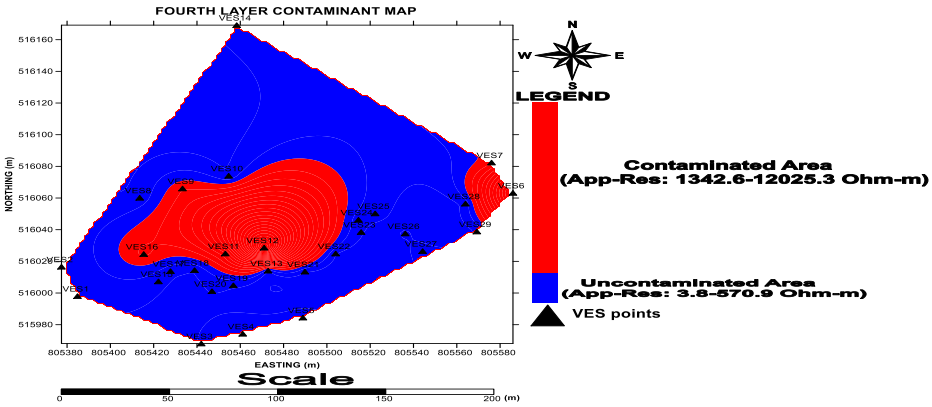

Figure 9b Spill site: Fourth layer contaminant map for VES 1-29

6. Conclusion

Geophysical assessment of the geological behavior of subsurface with hydrocarbon-embedded soil is to look for signatures of high electrical resistivity and evidence of a free contaminant zone just above the water table. In this study, the integrated method utilized reduced the uncertainties in the characterization of the site. The 2-dimensional resistivity imaging revealed the vertical and lateral extent where high resistive plumes were encountered, which are signatures of low conductive hydrocarbons. Vertical Electrical Sounding showed the depths the plumes have reached and uncontaminated zones. The impermeable clay seals the zones from contamination. Ground-Penetrating Radar identified the shadow zones where there are low reflections, which further confirmed the presence of plumes in the zone. Ground-Penetrating Radar signals terminate in a highly conductive zone. The study has shown the geological behavior of subsurface materials affected by hydrocarbon pollution and the importance of integrating different geophysical methods in geological site characterization of shallow subsurface pollution studies,

and the need for quick clean-up whenever there is spillage in an environment according to NUPRC (2002) guidelines.

REFERENCES

Agbonofo, J. 2009. Development as conflict: Ogoni move ment, the state and oil resources in Niger Delta, Nigeria, Doctoral Thesis Available (online) http://repub.eur.nl/res/pub/32647/90-423-03808_DOK/5B1/5D. Accessed 20 Dec 2024

AGI. Earth Imager 2013. 2-D, 3-D resistivity inversion software, version 1.5.10.Advanced Geosciences Inc., Austin. Available from https://www.agiusa.com/agi-earthimager-3d

Asseez, O.L. 1989. Review of the stratigraphy, sedimentation and structure of the Niger Delta. In: Kogbe (Ed.), Geology of Nigeria, Rock View (Nig.) Ltd., Jos, 311–324

Atekwana, E. et al. 2002. Geophysical investigation of vadose zone conductivity anomalies at a hydrocarbon contaminated site: implications for the assessment of intrinsic bioremediation. Jour. of environmental & engineering geophysics, vol. 7, no. 3, pp. 103-110.

Atekwana, E., Sauck, W., Werkema, D. 2000. Investigations of geoelectrical signatures at hydrocarbon contaminated site. Journal of Applied Geophysics. 44, 167 - 180.

Benard, J. 2023. Short note on the principles of geophysical methods for groundwater investigations. Retrieved July 7, 2023. Available from the link www.terraplus.com info@terraplus.com.

Bery, A.A. 2016. Slope monitoring study using soil mechanics properties and 4d electrical resistivity tomography methods. Soil Mechanics and Foundation Engineering, 53(1): 24-29.

Bodo, T., Lekpa, D. 2018. The petroleum exploitation and pollution in Ogoni, Rivers State, Nigeria: the community perspective. Eur Sci j;14(32):197. doi:10.19044/esj.2018.v14n32p197.

Bradford, J.H. 2003. GPR offset-dependent reflectivity analysis for characterization of a high-conductivity LNAPL plume, SAGEEP 2003 symposium on the application of geophysics to environmental and engineering problems: San antonio, tx, Env. Eng. geophys. Soc., p. 238-252.Available from: https://www.researchgate.net/publication/265160820_multioffset_gpr_methods_for_hyporheic_zone

Bradford, J.H. 2004. 3D Multi-offset, multi-polarization acquisition and processing of GPR data: A controlled NAPL spill experiment: sageep 2004 proceedings, symp. appl. geophys. Env. eng. prblm: colorado springs, co, env. eng. geophys. soc., 514-527.

De Vivo, B., Belkin, H.E., Lima, A. 2008. Environmental geochemistry: site characterization, data analysis and case histories. Elsevier, the Netherlands Linacre House, Jordan Hill, oxford ox2 8dp, uk

Delaney, A., Peapples, P., Arcone, S. 2001. Electrical resistivity of frozen and petroleum-contaminated fine-grained soil. cold regions science and technology 32: 107-119. Available from: https://www.sciencedirect.com/science/article/pii/s0165232x00000239

Doust H., Omatsola E., 1990. Niger Delta. in: edwards, j.d. and santogrossi, p.a., eds., divergent/passive margin basins, AAPG memoir 48, American association of petroleum geologists, Tulsa: 239-248

Everett, M. 2013. Near-Surface Applied Geophysics. Cambridge University press, 441 pp.

Eze S.U., Ogagarue, D.O., Nnorom, S.L., Osung, W.E., Ibitoye, T.A 2021. Integrated geophysical and geochemical methods for environmental assessment of subsurface hydrocarbon contamination: Environ Monit Assess. 193:451. https://doi.org/10.1007/s10661-021-09219-3.

Giadom, F.D., Akpokodje, E.G., Tse, A.C. 2015. Determination of migration rates of contaminants in a hydrocarbon-polluted site using non-reactive tracer test in the Niger Delta, Nigeria. Environmental earth sciences. 2015; doi.10.1007/s12665-015-4094-3.

Ideozu, R. U., Iheaturu, T. C., Ugwueze, C. U., et al. 2018. Reservoir properties and sealing potentials of the Akani Oil Field structures, Eastern Niger Delta Nigeria. Jour nal Oil Gas Petrochemistry Science, 1(2), 56–65. https:// doi.org/10.30881/jogps.00012

Ivanov, A. Y., Zatyagalova, V.V. 2008. A GIS approach to mapping oil spills in a marine environment. International Journal of Remote Sensing 29 (21): 6297 - 6313. Available from: https://doi.org/10.1080/01431160802175587

Lane, Jr, J.W. et al. 2004. Application of cross-borehole radar to monitor fieldscale vegetable oil injection experiments for biostimulation. symposium on the application of geophysics to engineering and environmental problems (SAGEEP), 22 to 26 February 2004, Colorado springs, Colorado, proceedings of environmental and engineering geophysical society, 20 p. Available from:https://www.growkudos.com/publications/10.4133%252f1.2923356.

Maury, A.P., Ronde, V., Fiandaca, G., Balbarini, N., Auken, E., Bjerg, P., Christiansen, A. 2017. Detailed landfill leachate plume mapping using 2d and 3d electrical resistivity tomography-with correlation to ionic strength measured in screens. Journal of Applied Geophysics., 138:1–8. Available from: https://www.researchgate.net/publication/312381885.

Nigerian Upstream Petroleum Regulatory Commission (NUPRC) 2002. Environmental Guidelines and Standards for the Petroleum Industry in Nigeria 1991 (Revised Edition); 2002 Available from:https://nesgroup.org/download_policy_drafts/Environmental%20Guidelines%20and%20Standards%20for%20the%20Petroleum%20Industry%20in%20Nigeria%20%28%20EGASPIN%29%20%282002%29%20Revised%20Edition_1661874693.pdf

Nwankwo, C.N., Emujakporue, G.O. 2012. Geophysical method of investigating groundwater and sub-soil contamination-a case study; American Journal of environmental engineering, 2(3):49–53 https://doi.org/10.5923/j.ajee. 20120203.02

Obasi, R.A., Balogun, O. 2001. Water quality and environmental impact assessment of water resources in Nigeria. African Journal of Environment Studies 2 (2) 228 – 231.

Okonny, I.P. 2002. Geology in Alagoa, E.J. and Derefaka, a (ed) the land and people of Rivers State, Eastern Niger Delta. Port Harcourt, Onyoma Research Publishers. 2002 [cited 2023 dec 30]

Olaojo, A.A., Oladunjoye, M.A., Sanuade, O.A. 2018. Geoelectrical assessment of polluted zone by sewage effluent in University of Ibadan campus Southwestern Nigeria. Environ monitoring assess 190:24. https://doi.org/10.1007/s10661-017-6389-1

Oyinkuro, O.A., Wariebi, K.A. 2017. Hydrocarbon spill site characterization by electrical resistivity tomography and ground penetrating radar methods - a review. Asian Journal of environment and ecology. 4(3): pp1-9.

Park, S. 2001. Site investigation technology of contaminated soil and groundwater. Journal of Korean Society of Agricultural Engineers 43 (6), 45 - 23.

Patel, S.K., Verma, P., Siggh, G.S. 2019. Agricultural growth and land use land cover change in peri-India, environmental monitoring and assessment.191;600. doi:10.100f/s 10661-019-7736-1.

Paterson, N. 1997. Remote mapping of mine wastes. in proceedings of exploration '97, fourth decennial international conference on mineral exploration, ed. A.G. Gubbins, 905-16. Toronto: prospectors and developers association of Canada.

Pazdirek, O., Blaha, V. 1996. Examples of resistivity imaging using multi electrode-100 resistivity field acquisition system. Eage 58th conference and technical exhibition extended Abstracts, Amsterdam.

Pomposiello, c. et al., 2004. resistivity imaging and ground penetrating radar survey at gualeguaychú landfill, entre ríos province, Argentina: evidence of a contamination plume. Iaga wg 1.2 on electromagnetic induction in the earth proceedings of the 17th workshop, Hyderabad, India.

Porsani, J.L. et al., 2004. The use of GPR and VES in delineating a contamination plume in a landfill site: a case study in SE Brazil. Journal of Applied geophysics. 55, no 3-4, pp. 199-209.

Rosales, R.M., Martinez-Pagan, P., Faz, A. 2012. Detecting underground storage tanks and contaminated areas in petrol stations by using 2D ERT. Near Surface Geophysics 12: 1 – 5

Sauck, W.A. et al. 1998. High conductivities associated with a LNAPL plume imaged by integrated geophysical techniques. Jour. of environ. and engineering geophysics, vol. 2, no. 3, pp. 203-212

Slater, I.D., Sandberg, S.K. 2000. Resistivity and induced polarization monitoring of salt transport under natural hydraulic gradients. Geophysics 65(2):408–420.

Tamuno, S., Felix, J.M. 2006. Crude oil resources: a blessing or curse to Nigeria – the case of the Niger Delta. Journal of research in national development 4(2): 53 – 58. Available from: https://www.ajol.info/index.php/jorind/article/view/42332\

Telford, W.M., Geldart, L.P., Sheriff, R.E 1990. Resistivity methods in: applied geophysics, 2nd edition, (Cambridge Univ. Press, Cambridge, uk) p 353–358. doi: https://doi.org/10.1017/cbo9781139167932.012

Uchegbulam, O., Ayolabi, E.A. 2014. Application of electrical resistivity imaging in investigating groundwater pollution in Sapele Area, Nigeria. Journal of water resource and protection.6:1369-1379. doi:10.4236/jwarp.2014.614126

UNDP (United Nations Development Programme). 2006. Niger delta human development report. P76, http://www.hdr.undp.org/en/ repor ts/national reports/ africa/ nigeria. Accessed 12 Sept 2023

United States Army Corps of Engineers (USACE) 1995. Geophysical exploration for engineering and environmental investigations. EM. 1110-1-1802. 208.

Werkema, D., Atekwana, E., Endres, A., Sauck, W., Cassidy, D. 2003. Investigating the geoelectrical response of hydrocarbon contamination undergoing biodegradation. geophysical research letters 30 (12), 1647. Available from: https://agupubs.onlinelibrary.wiley.com/doi/10.1029/2003gl017346.